Nonequilibrium characterization of equilibrium correlated quantum phases

Long Zhang,[1,2] Lin Zhang,[1,2] Ying Hu,[3,4] Sen Niu,[1,2] and Xiong-Jun Liu[1,2,5,*]

[1]*International Center for Quantum Materials and School of Physics, Peking University, Beijing 100871, China*
[2]*Collaborative Innovation Center of Quantum Matter, Beijing 100871, China*
[3]*State Key Laboratory of Quantum Optics and Quantum Optics Devices, Institute of Laser Spectroscopy, Shanxi University, Taiyuan, Shanxi 030006, China*
[4]*Collaborative Innovation Center of Extreme Optics, Shanxi University, Taiyuan 030006, China*
[5]*Institute for Quantum Science and Engineering and Department of Physics, Southern University of Science and Technology, Shenzhen 518055, China*

(Received 29 March 2019; revised 5 June 2021; accepted 8 June 2021; published 21 June 2021)

Quenching a quantum system involves three basic ingredients: the initial phase, the postquench target phase, and quantum dynamics, which may carry the information of the former two. Here we propose a dynamical theory, based on an interaction quench, to characterize both the equilibrium symmetry-breaking order and topological phases by nonequilibrium correlated quantum dynamics. We illustrate the theory with the Haldane-Hubbard model, which is quenched from an initial correlated magnetic phase to a topologically nontrivial regime. We show that the quench dynamics exhibit profound universal behaviors on the so-called band-inversion surfaces (BISs), from which both the topological phase in the weakly interacting regime and the correlated magnetic phase in the strongly interacting regime can be extracted. In particular, the topology is characterized by dynamical topological patterns emerging on BISs, which are robust against interaction-induced dephasing and heating; the symmetry-breaking order can be read out from a universal dynamical scaling behavior, which is valid beyond the mean-field theory. This work uncovers the first paradigm of nonequilibrium characterization of equilibrium symmetry-breaking and topological phases.

DOI: 10.1103/PhysRevB.103.224308

I. INTRODUCTION

The Landau symmetry-breaking phases and topological phases are two fundamental notions in condensed-matter physics. The equilibrium characterizations of the two types of phases are fundamentally different, respectively described by local orders [1] and nonlocal topological invariants [2–4] of many-body ground states, for which their experimental probes are also sharply distinct. Tuning a correlated system away from the equilibrium phase by, e.g., quenching leads to quantum dynamics which attracted lots of theoretical interest in recent years, with the research having been mainly focused on the fate of symmetry-breaking orders after quench, like the destruction of the equilibrium phases [5–7], and the emergence of dynamical phases [8]. Here we provide a perspective to consider how the far-from-equilibrium dynamics *encodes* the information of equilibrium quantum phases and raise a broad and intriguing issue—the nonequilibrium characterization of equilibrium symmetry-breaking and topological phases.

For noninteracting topological phases, the characterization by quantum dynamics has been actively studied in both theory [9–19] and experiment [20–25]. It was predicted that suddenly tuning a system from an initially trivial phase to a topological regime induces topological quench dynamics which links to and thus provides nonequilibrium characterization of the equilibrium topological phase of the postquench Hamiltonian [9–11]. The dynamical characterization provides conceptually new schemes to detect in experiment the topological phases with much higher precision compared with the equilibrium measurement strategies [9,21]. Nevertheless, so far the dynamical characterization theory has been developed for only noninteracting phases. For an interacting system with both the symmetry-breaking and topological phases, the quench dynamics are much more complicated due to the correlation effects [26,27]. How to develop a dynamical characterization theory for both the symmetry-breaking and topological phases is an open, although highly significant, question in both theory and experiment and an outstanding issue.

We address the issue and propose a dynamical characterization scheme via the spin-1/2 Haldane model [28,29] with Hubbard interaction, which hosts the magnetic phase and the topological phase in strongly and weakly interacting regimes, respectively [30–37]. The quench dynamics is induced by quenching the system from the initial symmetry-breaking phase with trivial topology to a target topological phase without symmetry breaking, i.e., across both the symmetry-breaking and topological phase transitions. The pseudospin quench dynamics follows a microscopic Landau-Lifshitz-Gilbert-Bloch equation, with the dephasing and heating effects being predicted. Importantly, we find that the correlated quench dynamics exhibits emergent robust topological patterns and a universal dynamical scaling on the one-dimensional (1D) momentum subspaces called band-inversion surfaces (BISs) [9], which characterize, respectively, the postquench topology and prequench magnetic

*Corresponding author: xiongjunliu@pku.edu.cn

orders. These exotic features manifest a profound dynamical bulk-surface correspondence relating equilibrium topology and symmetry-breaking orders to correlated quench dynamics on BISs.

II. INTERACTION QUENCH AND PSEUDOSPIN DYNAMICS

We consider the two-dimensional (2D) Haldane-Hubbard model, which can be realized in experiment [29] and characterized by the Hamiltonian

$$\begin{aligned} H &= H_0 + U\sum_{\vec{i}}(a^\dagger_{\vec{i}\uparrow}a^\dagger_{\vec{i}\downarrow}a_{\vec{i}\downarrow}a_{\vec{i}\uparrow} + b^\dagger_{\vec{i}\uparrow}b^\dagger_{\vec{i}\downarrow}b_{\vec{i}\downarrow}b_{\vec{i}\uparrow}),\\ H_0 &= -t_1\sum_{\langle\vec{i}\vec{j}\rangle,\sigma}(a^\dagger_{\vec{i}\sigma}b_{\vec{j}\sigma} + \text{H.c.}) - t_2\sum_{\langle\langle\vec{i}\vec{j}\rangle\rangle,\sigma}(e^{\mathrm{i}\phi}a^\dagger_{\vec{i}\sigma}a_{\vec{j}\sigma}\\ &\quad + e^{-\mathrm{i}\phi}b^\dagger_{\vec{i}\sigma}b_{\vec{j}\sigma} + \text{H.c.}) + M\sum_{\vec{i},\sigma}(a^\dagger_{\vec{i}\sigma}a_{\vec{i}\sigma} - b^\dagger_{\vec{i}\sigma}b_{\vec{i}\sigma}). \end{aligned} \tag{1}$$

Here $a_{\vec{i}\sigma}$ ($b_{\vec{i}\sigma}$) and $a^\dagger_{\vec{i}\sigma}$ ($b^\dagger_{\vec{i}\sigma}$) are annihilation and creation operators, respectively, for fermions of spin $\sigma = \uparrow,\downarrow$ on A (B) sites. The nearest-neighbor (t_1) and next-nearest-neighbor (t_2) hoppings are considered, with the latter having a phase $\pm\phi$. U is the on-site interaction, and M is an energy imbalance between the A and B sites. In Bloch momentum k space, the noninteracting Hamiltonian can be rewritten as $H_0 = \sum_{\mathbf{k},\sigma}\mathbf{h}(\mathbf{k})\cdot\boldsymbol{\tau}^\sigma$, where $\mathbf{h}(\mathbf{k}) = (h_x, h_y, h_z)$ mimics an effective Zeeman field [38], with the pseudospin operators $\tau^\sigma_z = a^\dagger_{\mathbf{k}\sigma}a_{\mathbf{k}\sigma} - b^\dagger_{\mathbf{k}\sigma}b_{\mathbf{k}\sigma}$, $\tau^\sigma_x = a^\dagger_{\mathbf{k}\sigma}b_{\mathbf{k}\sigma} + \text{H.c.}$, and $\tau^\sigma_y = -\mathrm{i}[\tau^\sigma_z, \tau^\sigma_x]$. It has been widely found [30–37] that in the ground state $|\Psi_{\text{GS}}\rangle$, an antiferromagnetic (AF) order $m_{\text{AF}} = (m_\downarrow - m_\uparrow)/2$ arises for strong repulsive interaction, and the energy imbalance M further leads to a charge order $m_{\text{C}} = (m_\uparrow + m_\downarrow)/2$ corrected by the Hubbard interaction, which characterizes the population difference in the two sublattices. Here the initial orders $m_\sigma \equiv \langle a^\dagger_{\vec{i}\sigma}a_{\vec{i}\sigma} - b^\dagger_{\vec{i}\sigma}b_{\vec{i}\sigma}\rangle U_{\text{in}}/4$, with U_{in} being the initial strong interaction and the expectation $\langle\cdot\rangle$ being computed in the ground state $|\Psi_{\text{GS}}\rangle$.

We consider the interaction quench from an initial magnetic phase in the strongly interacting regime ($U = U_{\text{in}} \gg t_1$) to a topologically nontrivial region in the weakly interacting regime ($U < t_1$) [Fig. 1(a)]. The quench dynamics corresponds to the time evolution of a given initial ground state under the postquench Hamiltonian. The initial ground state can be written down in the mean-field form $|\Psi_{\text{GS}}\rangle \to |\Psi_{\text{MF}}\rangle$, which solely depends on the order parameters [38], or as the Gutzwiller many-body wave function beyond the mean-field picture [39–42]. As studied below and detailed in the Supplemental Material [38], our central results are valid beyond the mean-field regime of the initial state. The time evolution of the many-body state under the weakly interacting postquench Hamiltonian can be investigated by the well-established flow equation method [43–46], with the details being summarized in Appendix A. Due to the interaction, the single-particle momentum is not conserved. However, we can investigate pseudospin dynamics in the projected momentum (k) space which is obtained by tracing out all other momenta of the many-body state, as shown in Figs. 1(b) and 1(c). The quench dynamics generically exhibit large-amplitude pseudospin

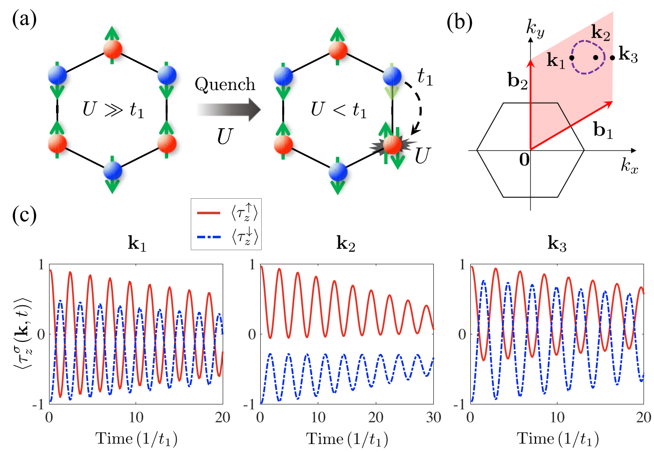

FIG. 1. Interaction quench and pseudospin dynamics. (a) The system undergoes a transition from an AF phase to a topologically nontrivial phase by quenching the interaction from $U \gg t_1$ to $U < t_1$. (b) The first Brillouin zone (hexagon) with the reciprocal-lattice vectors $\mathbf{b}_1 = \frac{2\pi}{3a_0}(\sqrt{3}, 1)$ and $\mathbf{b}_2 = \frac{4\pi}{3a_0}(0, 1)$ (a_0 is the lattice constant). The dashed purple line denotes the band-inversion surface of the spin-up component. (c) The pseudospin polarization $\langle\tau^\sigma_z\rangle$ oscillates after the quench for each spin $\sigma = \uparrow\downarrow$. Three points in the Brillouin zone in (b) are taken for example. Here $t_2 = 0.3t_1$, $M = -0.5t_1$, $m_{\text{C}} = 0.5t_1$, $m_{\text{AF}} = 4t_1$, and $U = 0.3t_1$ after quench.

oscillations only at momenta near the BIS (see the definition below). We then expect that universal behaviors of the correlated dynamics will emerge on the BIS which will link to both the prequench magnetic order and the postquench topology. In this study, we focus on quench dynamics in the early stage (up to a few oscillations), while long-time behaviors are not necessary for our purpose.

III. EQUATION OF MOTION

We first show that the essential physics of pseudospin dynamics can be captured by the equation of motion in the projected k space. Taking into account the dominating contributions from scattering, we obtain the following result (see the Supplemental Material [38] for derivation):

$$\frac{d\mathbf{S}_\sigma(t)}{dt} = \mathbf{S}_\sigma(t)\times 2\mathbf{h} - \eta^\sigma_1\mathbf{S}_\sigma(t)\times\frac{d\mathbf{S}_\sigma(t)}{dt} - \eta^\sigma_2\frac{\mathbf{S}_\sigma(t)}{T_{\text{g}}}, \tag{2}$$

where $\mathbf{S}_\sigma(\mathbf{k},t) \equiv \frac{1}{2}\langle\boldsymbol{\tau}^\sigma(\mathbf{k},t)\rangle$ ($\sigma = \uparrow,\downarrow$). The terms of the right-hand side have transparent physical interpretations. The first $2h$ term corresponds to the pseudospin precession induced by the single-particle Hamiltonian, while the second and third terms are induced by correlation effects. The η^σ_1 term represents the interaction-induced damping of precession, and the η^σ_2 term leads to heating, with $T_{\text{g}} \equiv 1/(2E_0)$ and $E_0(\mathbf{k}) = [h^2_x(\mathbf{k}) + h^2_y(\mathbf{k}) + h^2_z(\mathbf{k})]^{1/2}$. The heating reduces the length of the $\mathbf{S}_\sigma$ vector, while the damping drags the vector towards the $\mathbf{h}$ axis. This equation renders a mixed *microscopic* form of the Landau-Lifshitz-Gilbert [47] and Bloch [48] equations. Its form is not altered by characterizing the initial phase in the mean-field theory or as the Gutzwiller state, although the beyond-mean-field effects can correct the coefficients [38].

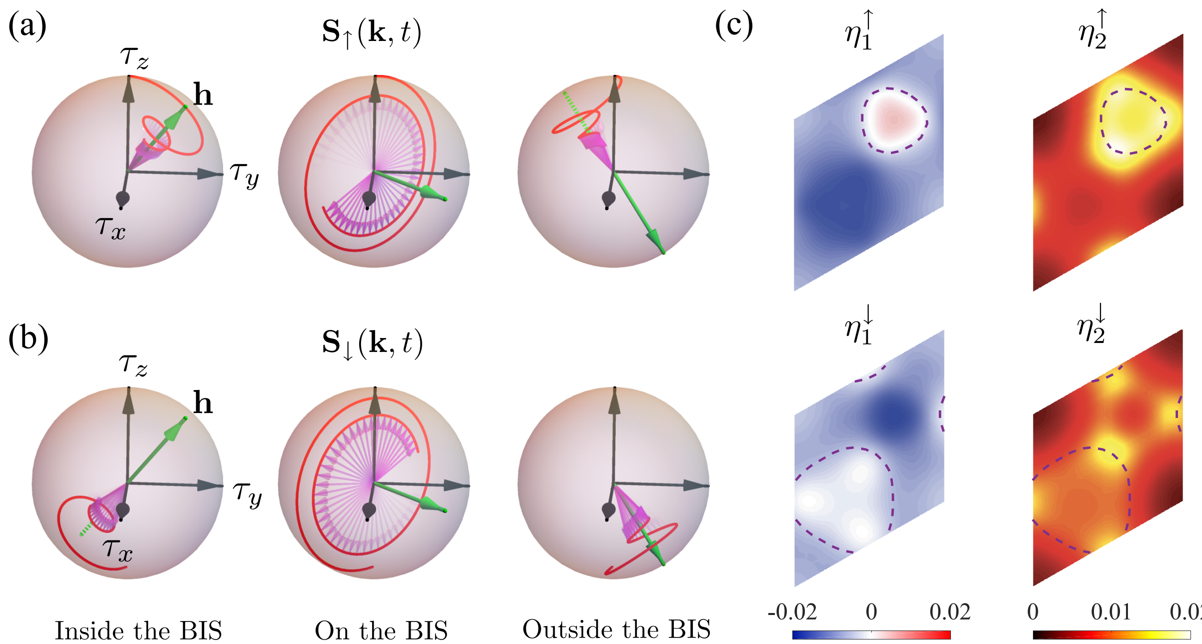

FIG. 2. Pseudospin dynamics from the equation of motion. Time evolution of pseudospin vectors for (a) spin up and (b) spin down. Damping and heating effects modify the precession, but to different degrees in different regions with respect to the BIS. (c) The calculated distribution of damping factors η_1^σ and heating factors η_2^σ. The dashed purple lines denote the *noninteracting* BISs for each spin. Here we take $t_2 = 0.3t_1$, $M = -0.5t_1$, $m_C = 0.5t_1$, $m_{AF} = 4t_1$, and the interaction $U = 0.3t_1$ after quench.

The solution up to the second order of postquench interaction U^2 reads

$$\mathbf{S}_\sigma(t) = \mathbf{S}_\sigma^{(0)} + \mathbf{S}_\sigma^{(c)}(t) + \mathbf{S}_\sigma^{(h)}(t) + \mathbf{S}_\sigma^{(l)}(t). \tag{3}$$

Here $\mathbf{S}_\sigma^{(0)} = [n_{+-}^\sigma(\mathbf{k}) - n_{--}^\sigma(\mathbf{k})]\mathbf{h}(\mathbf{k})/E_0(\mathbf{k})$ is a constant equaling the time-averaged value of the single-particle pseudospin procession and is proportional to the difference of the initial population in the upper (n_{+-}^σ) and lower (n_{--}^σ) eigenbands of the single-particle Hamiltonian, and $\mathbf{S}_\sigma^{(c)}(\mathbf{k},t) \sim \cos(t/T_g)$ is the single-particle oscillation around the averaged value $\mathbf{S}_\sigma^{(0)}$. The interaction corrects the pseudospin procession by inducing the high-frequency fluctuation $\mathbf{S}_\sigma^{(h)}(\mathbf{k},t) \approx -\lambda_1^\sigma(\mathbf{k},t)\mathbf{S}_\sigma^{(c)}(\mathbf{k},t)$, which reduces the pseudospin oscillation amplitude, and the low-frequency term $\mathbf{S}_\sigma^{(l)}(\mathbf{k},t) \approx -2\lambda_2^\sigma(\mathbf{k},t)\mathbf{h}(\mathbf{k})/E_0(\mathbf{k})$, which equilibrates the density distribution of the two eigenbands (embodied in λ_2^σ). The coefficients $\lambda_{1,2}^\sigma \propto U^2/E_0^2$ relate to the factors $\eta_{1,2}^\sigma$, as discussed below. Note that the entire many-body system evolves unitarily. The dephasing and heating arise in the projected quench dynamics at fixed k since all the particles with $k' \neq k$ act as a thermal bath scattering the k state.

The correlation effects can be better interpreted by examining the damping and heating effects on the single-particle BIS defined by $h_z(k) = 0$ in the Hamiltonian H_0 [9–11,21], which is a 1D momentum subspace with vanishing time-averaged spin polarization $\overline{S_\sigma(k,t)}|_{U=0} = \mathbf{S}_\sigma^{(0)}(\mathbf{k}) = 0$. On this BIS, we find $\eta_1^\sigma \simeq -4(d\lambda_2^\sigma/dt)T_g$ and $\eta_2^\sigma \simeq 4(d\lambda_1^\sigma/dt)T_g n_{+-}^\sigma n_{--}^\sigma$, where $d\lambda_{1,2}^\sigma/dt$ are approximately constant in the early stage of quench dynamics [38]. The former result of η_1^σ indicates that the damping effect on single-particle BISs is induced by density fluctuations (determined by λ_2^σ). Actually, if there is no interaction, the pseudospin vector S_σ on the BIS is always perpendicular to h, i.e., no dragging "force." The latter one of η_2^σ shows that the heating on BISs mainly results from the dephasing of the oscillation since the two eigenbands have been equally occupied [$n_{+-}^\sigma(\mathbf{k}) = n_{--}^\sigma(\mathbf{k})$]. Figure 2(c) shows the calculated distribution of $\eta_{1,2}^\sigma$. One can see that near the BISs (dashed lines), η_1^σ are small and the heating due to the η_2^σ term dominates the correlation effect. In comparison, the damping is enhanced at k away from the BIS. Hence, the damping and heating have different effects in different regions, leading to distinct precession dynamics [see Figs. 2(a) and 2(b)].

IV. CHARACTERIZATION BY EMERGENT TOPOLOGY

We show now that the correlated pseudospin dynamics on BISs exhibit robust emergent topological patterns which characterize the postquench topology. For noninteracting topological phases, a dynamical bulk-surface correspondence has been established [9–11], with the claim that the bulk topology can be characterized by a dynamical invariant defined on BISs, which reflects the total topological charges enclosed by all the BISs. Here the topological charge depicts the chirality of a monopole at the node of the spin-orbit field $h_{so}(k) \equiv (h_y, h_x)$, and their positions can be dynamically identified by the absence of oscillation after quench [10]. Now we generalize the dynamical characterization to the interacting regime.

From Eq. (2) we find that the interaction has different effects on the dynamical characterization of BISs and topological charges. Since the damping (η_1 term) modifies the procession, the BIS in the presence of interactions, determined by $\overline{S_\sigma(k,t)}|_{U\neq 0} = 0$, is deformed from the aforementioned single-particle BIS where h is perpendicular to S_σ. In contrast,

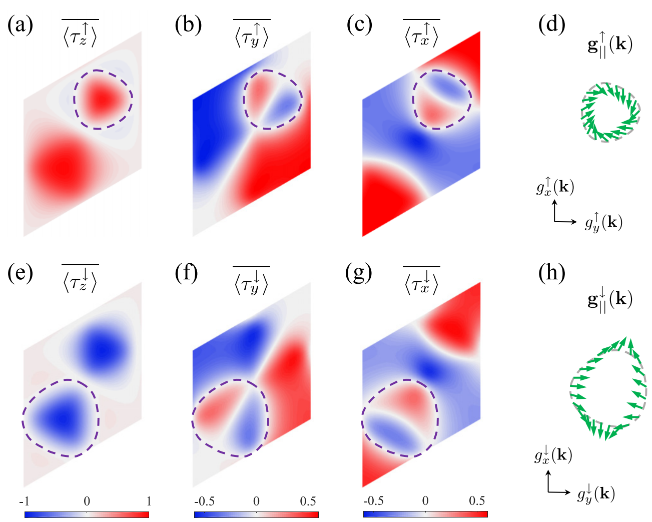

FIG. 3. Emergent topology of quench dynamics. (a) Time-averaged pseudospin textures $\overline{\langle\tau^{\uparrow}_{x,y,z}(\mathbf{k})\rangle}$ with (b) the corresponding projected dynamical field $\mathbf{g}^{\uparrow}_{\parallel}(\mathbf{k})$. (c) Time-averaged pseudospin textures $\overline{\langle\tau^{\downarrow}_{x,y,z}(\mathbf{k})\rangle}$ with (d) the corresponding projected dynamical field $\mathbf{g}^{\downarrow}_{\parallel}(\mathbf{k})$. The dashed lines denote the *interacting* BISs. The constructed dynamical field on the BIS for either spin characterizes the topology with Chern number $C = 1$. Here we take $t_2 = 0.3t_1$, $M = -0.5t_1$, $m_{\rm C} = 0.5t_1$, and $m_{\rm AF} = 4t_1$, and the postquench interaction $U = 0.3t_1$. The time average is taken over 5 times of the oscillation period for each $\mathbf{k}$.

one can easily prove that the dynamical identification of topological charges is immune to the interaction, for only heating has an effect at the momenta where $h_{\rm so}(k) = 0$. The dynamical topology of the correlated quench dynamics emerging on the BIS is dual to the topological charges enclosed by the BIS. Hence, we expect that the interaction may not induce a topological transition if the deformed BIS does not cross any topological charge, which is true for small η_1 near BISs [Fig. 2(c)].

We demonstrate the dynamical characterization in the interacting regime by numerics. A typical example is shown in Fig. 3, where we plot the time-averaged pseudospin textures $\overline{\langle\tau^{\sigma}_{x,y,z}(\mathbf{k})\rangle}$ for each spin $\sigma =\uparrow,\downarrow$. To characterize the topology, we introduce a dynamical field $\mathbf{g}^{\sigma}(\mathbf{k}) = \pm\frac{1}{\mathcal{N}_k}\partial_{k_\perp}\overline{S_\sigma(k,t)}$, with $+$ $(-)$ for $\sigma =\uparrow(\downarrow)$. Here the momentum $k_\perp$ is defined to be perpendicular to the BIS, and $\mathcal{N}_k$ is the normalization factor. Due to the damping and heating effects, the $\mathbf{g}^{\sigma}(\mathbf{k})$ vector is generally out of the x-y plane. We project the dynamical field onto the x-y plane, giving $\mathbf{g}^{\sigma}_{\parallel}(\mathbf{k}) = \hat{e}_{\parallel}\cdot\mathbf{g}^{\sigma}(\mathbf{k}) = (g^{\sigma}_y, g^{\sigma}_x)$, and find $\mathbf{g}^{\sigma}_{\parallel}(\mathbf{k}) \simeq \mathbf{h}_{\rm so}(\mathbf{k})$ on the interacting BISs (Appendix B). Therefore, the winding of $\mathbf{g}^{\sigma}_{\parallel}(\mathbf{k})$ on BIS quantifies the total topological charges enclosed by the BIS, corresponding to the topology of the postquench regime [Figs. 3(b) and 3(d)]. Note that this projection approach is different from the free-fermion regime, where the topology emerges in the bare dynamical field $g^{\sigma}(k)$ [9–11].

V. SYMMETRY-BREAKING ORDERS FROM QUENCH DYNAMICS

Finally, we show the highly nontrivial prediction that the prequench magnetic order can also be extracted from quench dynamics on BISs. The AF and charge orders characterize the spin and density distributions in A and B sites and thus are related to the pseudospin dynamics, in which the BISs play the pivotal role. We first consider the initial phase characterized by the mean-field theory that $|\Psi_{\rm GS}\rangle \to |\Psi_{\rm MF}\rangle$ and derive the magnetic order based on two considerations: (i) The BIS defined by $\overline{\mathbf{S}_\sigma(k,t)} = 0$ corresponds to the momenta satisfying $E_0^2(\mathbf{k}) + m_\sigma h_z(\mathbf{k}) = -(d\lambda_2^\sigma/dt)TE_0(\mathbf{k})E_0^\sigma(\mathbf{k})$, with $E_0^\sigma \equiv \sqrt{E_0^2 + 2m_\sigma h_z + m_\sigma^2}$. Here T is the interval for time averaging, and the right-hand side represents shift of BISs by interaction. This formula shows that the dynamical characterization of the BIS depends on both the prequench phase m_σ and the postquench Hamiltonian. (ii) The prequench magnetization directly determines the oscillation amplitude. We find that the half amplitude, defined as $Z_0^\sigma(\mathbf{k}) \equiv \langle\tau_z^\sigma(\mathbf{k}, t=0)\rangle$, reads $Z_0^\sigma = (d\lambda_2^\sigma/dt)Th_z/E_0 - m_\sigma(E_0^2 - h_z^2)/(E_0^2E_0^\sigma)$ on BISs. With the two results and up to the leading-order correction from the interaction, we obtain the scaling (see Appendix C)

$$f(m_\sigma) = -\frac{\mathrm{sgn}(Z_0^\sigma)}{g(Z_0^\sigma)} + O(U^4), \tag{4}$$

where $f(m_\sigma) = m_\sigma T_0$ and $g(Z_0^\sigma) = \sqrt{1 - Z_0^{\sigma\,2}}/\pi$, with $T_0(\mathbf{k}) = \pi/E_0$. The result in Eq. (4) gives a universal scaling at any k on BISs and is insensitive to interactions.

We emphasize that the scaling in Eq. (4) is satisfied beyond the mean-field theory. For the initial phase described by the correlated Gutzwiller wave function $|\Psi_{\rm GS}\rangle \to |\Psi_{\rm G}\rangle$ (Appendix D), the same scaling holds, with Z_0^σ and the order parameters m_σ being now renormalized by correlations in the more precise Gutzwiller ground state. The broad validity beyond the mean-field description stems from the dynamical symmetry between the two eigenbands. By definition, on the BIS, the populations in the two eigenbands are equal $[n^\sigma_{+-}(\mathbf{k}) \simeq n^\sigma_{--}(\mathbf{k})]$. and the pseudospin dynamics is resonant. As a result, the asymmetric beyond-mean-field corrections coming from different scattering channels cancel out on the BIS, making the scaling law solely dependent on the renormalized order parameters. The details are given in the Supplemental Material [38].

We provide numerical results in Fig. 4(a) for the spin-up component. By identifying the BIS (the dashed purple curve), we record the short-time dynamics at momenta of three kinds: inside ($\mathbf{k}_1^<$), outside ($\mathbf{k}_1^>$), and right on the BIS ($\mathbf{k}^=_{1,2,3}$). We measure both $Z_0(k)$ and $T_0(k)$ versus order parameters $m_\uparrow/t_1$ [Fig. 4(b)]. The results are plotted as points $(|m_\uparrow T_0|, \sqrt{1 - Z_0^2})$ in Fig. 4(c), showing that the data measured on the BIS all satisfy the scaling. In experiment, one can obtain m_σ by measuring only the first one or two oscillations, i.e., the short-term dynamics. The AF order is then given by $m_{\rm AF} = (m_\downarrow - m_\uparrow)/2$, and the charge order $m_{\rm C} = (m_\uparrow + m_\downarrow)/2$.

VI. CONCLUSION AND DISCUSSION

The universal scaling and the dynamical topology of the quench dynamics emerging on BISs unveil a profound dynamical bulk-surface correspondence for both the topology and symmetry-breaking orders. This correspondence is obtained

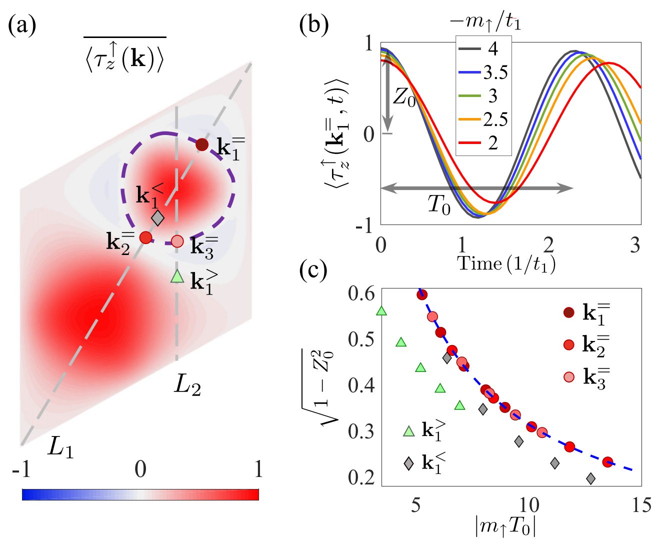

FIG. 4. Characterizing symmetry-breaking order. (a) The momenta taken for measurement. Three points lie on the BIS, with $\mathbf{k}_{1,2}^{=}$ being in line L_1, $(k_x, k_y) = \mathbf{b}_1 + \mathbf{b}_2$, and $\mathbf{k}_3^{=}$ being in line L_2, $k_x = \frac{4\pi}{9a_0}\sqrt{3}$. One is chosen inside the BIS with $\mathbf{k}_1^{<} = \frac{3}{5}(\mathbf{b}_1 + \mathbf{b}_2)$, and one is outside the BIS with $\mathbf{k}_1^{>} = \frac{2}{3}\mathbf{b}_1 + \frac{1}{3}\mathbf{b}_2$. (b) Both the half oscillation amplitude Z_0 and the oscillation period T_0 are measured for different magnetizations $m_\uparrow/t_1 = -\{2, 2.5, 3, 3.5, 4\}$. (c) The numerical results are shown as $(|m_\uparrow T_0|, \sqrt{1 - Z_0^2})$. The data taken on the BIS all satisfy the function $f(x) = \pi/x$ (dashed blue curve), which verifies the relation of Eq. (4). Here we take $t_2 = 0.3t_1$, $M = -0.5t_1$, and the postquench interaction $U = 0.3t_1$.

when the system is quenched across both the topological and conventional symmetry-breaking phase transitions, in sharp contrast to the conventional studies of quantum quenches across only the conventional phase transition [5–7] or the topological transition [9–19]. In particular, the quench dynamics for the symmetry-breaking phase without combining it with the topological transition exhibits no such universal scaling since the BISs emerge dynamically only for the quenches across the topological transition, showing the importance of BISs in the nonequilibrium characterization of both the topological and symmetry-breaking phases. Further, while here we consider the Haldane-Hubbard model, the main results are broadly applicable to generic 2D Chern-Hubbard insulators and 1D topological-Hubbard systems as well. Thus, this work opens an avenue toward the unified characterization of symmetry-breaking and topological phases by quench dynamics.

Aside from the theoretical aspects, the present dynamical characterization theory provides high-precision approaches with experimental feasibility to detect correlated phases. First of all, this characterization theory simplifies the strategy by measuring the quench dynamics only on the BIS which is a lower-dimensional momentum subspace. Second, by definition the quantum (pseudo)spin dynamics is resonant on BISs; hence, the dynamical behaviors are easily resolved in experiment. Finally, the short-term quench dynamics already provides sufficient information to characterize both the pre- and postquench phases, which is generically not affected by detrimental effects like thermal effects. This leads to the high-precision measurement which can be achieved in current experiments. Particularly, the dynamical characterization of noninteracting topological phases has been experimentally realized in both ultracold atoms [21,23] and solid-state spin systems [24,25]. The Haldane model has been realized in ultracold atoms [29], the interaction quench can be implemented via Feshbach resonance [49], and the quench-induced pseudospin dynamics can be measured by the tomography of Bloch states [50,51].

ACKNOWLEDGMENTS

This work was supported by the National Natural Science Foundation of China (Grants No. 11825401, No. 11761161003, No. 11921005, and No. 11874038), the National Key R&D Program of China (Grants No. 2016YFA0301604 and No. 2017YFA0304203), and the Strategic Priority Research Program of the Chinese Academy of Sciences (Grant No. XDB28000000). Y.H. also acknowledges support from National Thousand-Young-Talents Program and Changjiang Scholars and Innovative Research Team (Grant No. IRT13076).

APPENDIX A: FLOW EQUATION METHOD

The process of applying the Flow equation method is summarized as follows. First, through a unitary transformation that changes continuously with a flow parameter l, we (nearly) diagonalize the postquench Hamiltonian at $l \to \infty$ [46]. Accordingly, the transformation of an operator $\mathcal{O}(l)$ (including the Hamiltonian) follows the flow equation $d\mathcal{O}(l)/dl = [\eta(l), \mathcal{O}(l)]$, where the canonical generator $\eta(l) = [H_0(l), H_I(l)] = -\eta(l)^\dagger$ is anti-Hermitian, with H_I being the interacting term of the full Hamiltonian. Second, the time-evolved operator $\mathcal{O}(l \to \infty, t)$ is obtained straightforwardly in the diagonal bases. Finally, we perform the backward transformation so that the operator flows back as $\mathcal{O}(l \to \infty, t) \to \mathcal{O}(0, t)$ [52,53]. The dynamical evolution is then given in the original bases.

For the present system, we consider the ansatz

$$H(l) = \sum_{\mathbf{k},\sigma,s=\pm} \mathcal{E}_s(\mathbf{k}){:}c^\dagger_{\mathbf{k},s\sigma} c_{\mathbf{k},s\sigma}{:} + \sum_{\substack{\mathbf{p}'\mathbf{p}\mathbf{q}'\mathbf{q}\\ s_1s_2s_3s_4}} U^{s_1s_2s_3s_4}_{\mathbf{p}'\mathbf{p}\mathbf{q}'\mathbf{q}}(l){:}c^\dagger_{\mathbf{p}',s_1\uparrow} c_{\mathbf{p},s_2\uparrow} c^\dagger_{\mathbf{q}',s_3\downarrow} c_{\mathbf{q},s_4\downarrow}{:}, \quad \text{(A1)}$$

where $\mathcal{E}_\pm(\mathbf{k})$ are the band energies of H_0, the normal ordering is with respect to the initial state $|\Psi_{\rm GS}\rangle$, and $c^\dagger_{\mathbf{k},\pm\sigma}$ ($c_{\mathbf{k},\pm\sigma}$) are the creation (annihilation) operators of spin $\sigma = \uparrow\downarrow$ for the upper and lower band states of H_0 [38]. The interaction strength $U^{s_1s_2s_3s_4}_{\mathbf{p}'\mathbf{p}\mathbf{q}'\mathbf{q}}(l)$ is defined for momentum-conserved scattering channels. With the interaction weaker than the bandwidth, only the leading-order contributions from scatterings up to U^2 will be considered. With the previously defined canonical generator $\eta(l)$, the interaction $U(l)$ decays exponentially with l and flows to zero at $l \to \infty$. We then work out the flow of creation and annihilation operators with respect to the A and B sites, with $\mathcal{A}^\dagger_{\mathbf{k}\uparrow}(l=0) = a^\dagger_{\mathbf{k}\uparrow}$ and $\mathcal{B}^\dagger_{\mathbf{k}\uparrow}(l=0) = b^\dagger_{\mathbf{k}\uparrow}$, from the same generator $\eta(l)$. Finally, since the single-particle momentum is not conserved, we obtain the time evolution of the pseudospin polarization at each projected momentum k: $\langle\tau_z^\sigma(\mathbf{k},t)\rangle = \langle\Psi_{\rm GS}|\mathcal{A}^\dagger_{\mathbf{k}\sigma}(l=0,t)\mathcal{A}_{\mathbf{k}\sigma}(l=0,t) - \mathcal{B}^\dagger_{\mathbf{k}\sigma}(l=0,t)\mathcal{B}_{\mathbf{k}\sigma}(l=0,t)|\Psi_{\rm GS}\rangle$, similar to that for $\langle\tau^\sigma_{x,y}(\mathbf{k},t)\rangle$.

APPENDIX B: DYNAMICAL CHARACTERIZATION OF TOPOLOGY

The time-averaged pseudospin textures in the presence of interaction are $\overline{\langle\tau_i^\sigma\rangle} = \langle\tau_i^{\sigma(0)}\rangle + \overline{\langle\tau_i^{\sigma(l)}\rangle} = \frac{h_i}{E_0}[n^\sigma_{+-}(\mathbf{k}) - n^\sigma_{--}(\mathbf{k}) - \frac{d\lambda_2^\sigma(\mathbf{k})}{dt}T]$ $(i = x, y, z)$, where T is the period over which the time average is taken and $\lambda_2^\sigma \propto U^2$ represents the interaction shift [38]. Here $n^\sigma_{\pm-}(\mathbf{k}) = \frac{1}{2} \mp \frac{E_0^2+m_\sigma h_z}{2E_0E_0^\sigma}$ are the populations of the initial ground state projected onto the upper (n^σ_{+-}) and lower (n^σ_{--}) bands of the single-particle Hamiltonian. The BIS is determined by $\overline{\langle\tau_i^\sigma(\mathbf{k})\rangle} = 0$, which leads to

$$\delta n_I^\sigma(\mathbf{k}) \equiv n^\sigma_{+-}(\mathbf{k}) - n^\sigma_{--}(\mathbf{k}) - \frac{d\lambda_2^\sigma(\mathbf{k})}{dt}T = 0. \qquad \text{(B1)}$$

Note that in the interacting system, $k_\perp$ is defined to be perpendicular to the contour of $\delta n_I^\sigma(\mathbf{k})$. For the contours infinitely close to $\delta n_I^\sigma(\mathbf{k}_0) = 0$, we have $\delta n_I^\sigma(\mathbf{k}_0 \pm \hat{e}_\perp k_\perp) \simeq \pm c_I k_\perp/E_0$, with c_I being a coefficient dependent on m_σ, U, and T. Therefore, we have

$$\partial_{k_\perp}\overline{\langle\tau_i^\sigma\rangle} = \lim_{k_\perp\to 0}\frac{1}{2k_\perp}\left[\frac{h_i}{E_0^2}\delta n_I^\sigma(\mathbf{k}_0 + \hat{e}_\perp k_\perp) - \frac{h_i}{E_0}\delta n_I^\sigma(\mathbf{k}_0 - \hat{e}_\perp k_\perp)\right] = c_I\frac{h_i}{E_0^2}, \qquad \text{(B2)}$$

which means that the dynamical field $\partial_{k_\perp}\overline{\langle\boldsymbol{\tau}^\sigma\rangle}$ on the (interacting) BIS characterizes the vector field $\mathbf{h}(\mathbf{k})$ despite the interaction effect. Due to the AF order, quenches for the two spins $\sigma = \uparrow\downarrow$ are along opposite directions. Thus, according to Ref. [9], we define the projected dynamical fields on the BIS $\mathbf{g}^\sigma_\parallel(\mathbf{k}) = (g^\sigma_y, g^\sigma_x)$ with components given by $g^\sigma_{y,x}(\mathbf{k}) = \pm\frac{1}{\mathcal{N}_k}\partial_{k_\perp}\overline{\langle\tau^\sigma_{y,x}\rangle}$. Here the $+$ $(-)$ sign is for $\sigma = \uparrow$ $(\downarrow)$, and $\mathcal{N}_k$ is the normalization factor. The topological invariant is then defined by the winding of the projected dynamical field with $\sigma = \uparrow$ or $\downarrow$:

$$w = \sum_j \frac{1}{2\pi}\int_{\mathrm{BIS}_j}\left[g^\sigma_y(\mathbf{k})dg^\sigma_x(\mathbf{k}) - g^\sigma_x(\mathbf{k})dg^\sigma_y(\mathbf{k})\right]. \qquad \text{(B3)}$$

APPENDIX C: UNIVERSAL SCALING BEHAVIOR

In the presence of interaction, the BIS is given by Eq. (B1). We assume $|d\lambda_2^\sigma/dt|T \ll 1$. We regard the interaction effect as a perturbation and approximate m_σ and h_z to the first order of $\varepsilon \equiv T d\lambda_2^\sigma/dt$, i.e., $m_\sigma = m_\sigma^{(0)} + \varepsilon m_\sigma^{(1)}$ and $h_z = h_z^{(0)} + \varepsilon h_z^{(1)}$. Calculations yield $m_\sigma^{(0)} = -\mathrm{sgn}(Z_0^\sigma)E_0/\sqrt{1 - Z_0^{\sigma\,2}}$ and $m_\sigma^{(1)} = 0$. To the second order of U, we obtain the universal scaling behavior shown in Eq. (4).

APPENDIX D: GUTZWILLER GROUND STATE

We take the Gutzwiller ansatz

$$|\Psi_{\rm G}\rangle = \prod_i(1 - \alpha A_i)(1 - \alpha B_i)|\Psi_{\rm MF}\rangle, \qquad \text{(D1)}$$

where α is the variational parameter with $0 \leqslant \alpha \leqslant 1$. Here $A_i \equiv a^\dagger_{i\uparrow}a^\dagger_{i\downarrow}a_{i\downarrow}a_{i\uparrow}$, $B_i \equiv b^\dagger_{i\uparrow}b^\dagger_{i\downarrow}b_{i\downarrow}b_{i\uparrow}$, and $|\Psi_{\rm MF}\rangle$ is the mean-field ground state. We rewrite the wave function into the momentum space and keep the leading-order terms. The constructed wave function is the correlated many-body state, given by the superposition of the mean-field state and a series of excited states via the leading-order scatterings [38]. With this, we find that the equation of motion keeps the same form as Eq. (2), but the parameters are renormalized by the interaction, and more importantly, the quench dynamics beyond the mean-field picture still exhibits the same universal scaling on the BIS.

[1] L. D. Landau, On the theory of phase transitions, in *Collected Papers of L. D. Landau* (Elsevier, 2013), Chap. 29, pp. 193–216.
[2] M. Z. Hasan and C. L. Kane, Colloquium: Topological insulators, Rev. Mod. Phys. **82**, 3045 (2010).
[3] X. L. Qi and S. C. Zhang, Topological insulators and superconductors, Rev. Mod. Phys. **83**, 1057 (2011).
[4] X. G. Wen, Topological orders in rigid states, Int. J. Mod. Phys. B **4**, 239 (1990).
[5] N. Tsuji, M. Eckstein, and P. Werner, Nonthermal Antiferromagnetic Order and Nonequilibrium Criticality in the Hubbard Model, Phys. Rev. Lett. **110**, 136404 (2013).
[6] M. S. M. Fabrizio, Nonequilibrium dynamics in the antiferromagnetic Hubbard model, Phys. Rev. B **88**, 165113 (2013).
[7] K. Balzer, F. A. Wolf, I. P. McCulloch, P. Werner, and M. Eckstein, Nonthermal Melting of Néel Order in the Hubbard Model, Phys. Rev. X **5**, 031039 (2015).
[8] M. S. Foster, M. Dzero, V. Gurarie, and E. A. Yuzbashyan, Quantum quench in a $p + ip$ superfluid: Winding numbers and topological states far from equilibrium, Phys. Rev. B **88**, 104511 (2013).
[9] L. Zhang, L. Zhang, S. Niu, and X.-J. Liu, Dynamical classification of topological quantum phases, Sci. Bull. **63**, 1385 (2018).
[10] L. Zhang, L. Zhang, and X.-J. Liu, Dynamical detection of topological charges, Phys. Rev. A **99**, 053606 (2019).
[11] L. Zhang, L. Zhang, and X.-J. Liu, Characterizing topological phases by quantum quenches: A general theory, Phys. Rev. A **100**, 063624 (2019).
[12] C. Wang, P. Zhang, X. Chen, J. Yu, and H. Zhai, Scheme to Measure the Topological Number of a Chern Insulator from Quench Dynamics, Phys. Rev. Lett. **118**, 185701 (2017).
[13] J. Yu, Measuring Hopf links and Hopf invariants in a quenched topological Raman lattice, Phys. Rev. A **99**, 043619 (2019).
[14] M. McGinley and N. R. Cooper, Topology of One-Dimensional Quantum Systems Out of Equilibrium, Phys. Rev. Lett. **121**, 090401 (2018).
[15] X.-L. Yu, L. Zhang, J. Wu, and X.-J. Liu, Quantum Dynamical Characterization and Simulation of Topological Phases with High-Order Band Inversion Surfaces, Phys. Rev. X Quantum **2**, 020320 (2021).

[16] L. Li, W. Zhu, and J. Gong, Direct dynamical characterization of higher-order topological phases with nested band inversion surfaces, Sci. Bull., doi: 10.1016/j.scib.2021.04.006.

[17] H. Hu and E. Zhao Topological Invariants for Quantum Quench Dynamics from Unitary Evolution, Phys. Rev. Lett. **124**, 160402 (2020).

[18] B. Zhu, Y. Ke, H. Zhong, and C. Lee, Dynamic winding number for exploring band topology, Phys. Rev. Res. **2**, 023043 (2020).

[19] L. Zhang, L. Zhang, and X.-J. Liu, Unified Theory to Characterize Floquet Topological Phases by Quench Dynamics, Phys. Rev. Lett. **125**, 183001 (2020).

[20] B. Song, L. Zhang, C. He, T. F. J. Poon, E. Hajiyev, S. Zhang, X.-J. Liu, and G.-B. Jo, Observation of symmetry-protected topological band with ultracold fermions, Sci. Adv. **4**, eaao4748 (2018).

[21] W. Sun, C.-R. Yi, B.-Z. Wang, W.-W. Zhang, B. C. Sanders, X.-T. Xu, Z.-Y. Wang, J. Schmiedmayer, Y. Deng, X.-J. Liu, S. Chen, and J.-W. Pan, Uncover Topology by Quantum Quench Dynamics, Phys. Rev. Lett. **121**, 250403 (2018).

[22] M. Tarnowski, F. N. Ünal, N. Fläschner, B. S. Rem, A. Eckardt, K. Sengstock, and C. Weitenberg, Measuring topology from dynamics by obtaining the Chern number from a linking number, Nat. Commun. **10**, 1728 (2019).

[23] C.-R. Yi, L. Zhang, L. Zhang, R.-H. Jiao, X.-C. Cheng, Z.-Y. Wang, X.-T. Xu, W. Sun, X.-J. Liu, S. Chen, and J.-W. Pan, Observing Topological Charges and Dynamical Bulk-Surface Correspondence with Ultracold Atoms, Phys. Rev. Lett. **123**, 190603 (2019).

[24] Y. Wang, W. Ji, Z. Chai, Y. Guo, M. Wang, X. Ye, P. Yu, L. Zhang, X. Qin, P. Wang, F. Shi, X. Rong, D. Lu, X.-J. Liu, and J. Du, Experimental observation of dynamical bulk-surface correspondence for topological phases, Phys. Rev. A **100**, 052328 (2019).

[25] W. Ji, L. Zhang, M. Wang, L. Zhang, Y. Guo, Z. Chai, X. Rong, F. Shi, X.-J. Liu, Y. Wang, and J. Du, Quantum Simulation for Three-Dimensional Chiral Topological Insulator, Phys. Rev. Lett. **125**, 020504 (2020).

[26] J. Eisert, M. Friesdorf, and C. Gogolin, Quantum many-body systems out of equilibrium, Nat. Phys. **11**, 124 (2015).

[27] T. Giamarchi, A. J. Millis, O. Parcollet, H. Saleur, and L. F. Cugliandolo, *Strongly Interacting Quantum Systems out of Equilibrium* (Oxford University Press, Oxford, 2016).

[28] F. D. M. Haldane, Model for a Quantum Hall Effect without Landau Levels: Condensed-Matter Realization of the "Parity Anomaly," Phys. Rev. Lett. **61**, 2015 (1988).

[29] G. Jotzu, M. Messer, R. Desbuquois, M. Lebrat, T. Uehlinger, D. Greif, and T. Esslinger, Experimental realization of the topological Haldane model with ultracold fermions, Nature (London) **515**, 237 (2014).

[30] C. Hickey, P. Rath, and A. Paramekanti, Competing chiral orders in the topological Haldane-Hubbard model of spin-$\frac{1}{2}$ fermions and bosons, Phys. Rev. B **91**, 134414 (2015).

[31] W. Zheng, H. Shen, Z. Wang, and H. Zhai, Magnetic-order-driven topological transition in the Haldane-Hubbard model, Phys. Rev. B **91**, 161107(R) (2015).

[32] X.-J. Liu, Z.-X. Liu, K. T. Law, W. V. Liu, and T. K. Ng, Chiral topological orders in an optical Raman lattice, New J. Phys. **18**, 035004 (2016).

[33] V. S. Arun, R. Sohal, C. Hickey, and A. Paramekanti, Mean field study of the topological Haldane-Hubbard model of spin-$\frac{1}{2}$ fermions, Phys. Rev. B **93**, 115110 (2016).

[34] C. Hickey, L. Cincio, Z. Papić, and A. Paramekanti, Haldane-Hubbard Mott Insulator: From Tetrahedral Spin Crystal to Chiral Spin Liquid, Phys. Rev. Lett. **116**, 137202 (2016).

[35] T. I. Vanhala, T. Siro, L. Liang, M. Troyer, A. Harju, and P. Törmä, Topological Phase Transitions in the Repulsively Interacting Haldane-Hubbard Model, Phys. Rev. Lett. **116**, 225305 (2016).

[36] J. Wu, J. P. L. Faye, D. Sénéchal, and J. Maciejko, Quantum cluster approach to the spinful Haldane-Hubbard model, Phys. Rev. B **93**, 075131 (2016).

[37] A. Rubio-García and J. J. García-Ripoll, Topological phases in the Haldane model with spin-spin on-site interactions, New J. Phys. **20**, 043033 (2018).

[38] See Supplemental Material at http://link.aps.org/supplemental/10.1103/PhysRevB.103.224308 for more details of (i) the Haldane model and mean-field ground state, (ii) flow equations, (iii) equation of motion, (iv) dynamical characterization, and (v) results beyond mean-field theory, which includes Figs. S1–S3 and Refs. [28,39–42,52–54].

[39] M. C. Gutzwiller, Effect of Correlation on the Ferromagnetism of Transition Metals, Phys. Rev. Lett. **10**, 159 (1963).

[40] M. C. Gutzwiller, Correlation of electrons in a narrow *s* band, Phys. Rev. **137**, A1726 (1965).

[41] Y. M. Li and N. d'Ambrumenil, A new expansion for generalized Gutzwiller wave functions: Antiferromagnetic case, J. Appl. Phys. **73**, 6537 (1993).

[42] D. Eichenberger and D. Baeriswyl, Superconductivity and antiferromagnetism in the two-dimensional Hubbard model: A variational study, Phys. Rev. B **76**, 180504(R) (2007).

[43] S. D. Glazek and K. G. Wilson, Renormalization of Hamiltonians, Phys. Rev. D **48**, 5863 (1993).

[44] S. D. Glazek and K. G. Wilson, Perturbative renormalization group for Hamiltonians, Phys. Rev. D **49**, 4214 (1994).

[45] F. Wegner, Flow-equations for Hamiltonians, Ann. Phys. (Berlin) **506**, 77 (1994).

[46] S. Kehrein, *The Flow Equation Approach to Many-Particle Systems* (Springer, Berlin, 2006).

[47] T. L. Gilbert, A phenomenological theory of damping in ferromagnetic materials, IEEE Trans. Magn. **40**, 3443 (2004).

[48] F. Bloch, Nuclear induction, Phys. Rev. **70**, 460 (1946).

[49] C. Chin, R. Grimm, P. Julienne, and E. Tiesinga, Feshbach resonances in ultracold gases, Rev. Mod. Phys. **82**, 1225 (2010).

[50] P. Hauke, M. Lewenstein, and A. Eckardt, Tomography of Band Insulators from Quench Dynamics, Phys. Rev. Lett. **113**, 045303 (2014).

[51] N. Fläschner, B. S. Rem, M. Tarnowski, D. Vogel, D.-S. Lühmann, K. Sengstock, and C. Weitenberg, Experimental reconstruction of the Berry curvature in a Floquet Bloch band, Science **352**, 1091 (2016).

[52] M. Moeckel and S. Kehrein, Interaction Quench in the Hubbard Model, Phys. Rev. Lett. **100**, 175702 (2008).

[53] M. Moeckel and S. Kehrein, Real-time evolution for weak interaction quenches in quantum systems, Ann. Phys. (NY) **324**, 2146 (2009).

[54] J. J. Sakurai, *Modern Quantum Mechanics* (Addison-Wesley, Reading, MA, 1994), Chap. 5.